Selected Paper

μ-Acetato-di-μ-phenolato-metal(II)cobalt(II) (Metal = Fe, Co, Ni, Cu, Zn) Complexes with Low-Spin Co(II): Synthesis, Structures, and Magnetism

Kohta Matsumoto, Noboru Sekine, Keisuke Arimura, Masaaki Ohba,† Hiroshi Sakiyama,[1] and Hisashi Ōkawa*

Department of Chemistry, Faculty of Science, Kyushu University, Hakozaki 6-10-1, Higashi-ku, Fukuoka 812-8581

[1]Department of Material and Biological Chemistry, Faculty of Science, Yamagata University, Kojirokawa, Yamagata 990-8560

Received December 25, 2003; E-mail: okawascc@mbox.nc.kyushu-u.ac.jp

The dinucleating macrocyclic ligand $(L^{2;2})^{2-}$, prepared by the [1:1] cyclic condensation of *N*,*N*′-dimethyl-*N*,*N*′-ethylenedi(5-bromo-3-formyl-2-hydroxybenzylamine) and ethylenediamine, has dissimilar $N(amine)_2O_2$ and $N(imine)_2O_2$ metal-binding sites sharing two phenolic oxygen atoms. It has afforded μ-acetato-di-μ-phenolato-metal(II)cobalt(II) complexes (metal(II) = Fe^{II}, Co^{II}, Ni^{II}, Cu^{II}, Zn^{II}). X-ray crystallographic studies indicate that the M^{II} is bound to the $N(amine)_2O_2$ site and has a square-pyramidal geometry with an acetate oxygen at the axial site. The Co^{II} bound to the $N(imine)_2O_2$ site has a square-pyramidal geometry with an acetate oxygen at the apex or a distorted octahedral geometry with further coordination of a methanol molecule. The Co^{II} in the $N(imine)_2O_2$ site is of low-spin and has one unpaired electron in its d_{z^2} orbital. Magnetic studies indicate an antiferromagnetic interaction in the FeCo and CoCo complexes whereas a ferromagnetic interaction in the NiCo and CuCo complexes. The magnetic properties of the complexes are discussed in terms of the electronic structure of the M^{II} ion and the dinuclear MCo core structure.

Magnetic studies of heterodinuclear complexes are important for inspecting the spin-exchange mechanism with respect to the electronic structures of the interacting metal ions.[1] Extensive studies of di-μ-phenolato-copper(II)metal(II) complexes[1–8] have shown that an antiferromagnetic interaction occurs within the molecule when the M^{II} has unpaired electron in its $d_{x^2-y^2}$ orbital, whereas a ferromagnetic interaction occurs when the M^{II} has unpaired electron(s) in d orbital(s) other than $d_{x^2-y^2}$ orbital (*x* and *y* axes are taken along donor atoms on the equatorial plane). The ferromagnetic interaction in the latter case is explained by the strict orthogonality of magnetic orbitals.[1,4]

Low-spin Co^{II} has one unpaired electron in either d_{z^2} orbital or d_{xz} (d_{yz}) orbital.[9] It is of interest to study magnetic interaction in heterodinuclear M^{II}–Co^{II} ($S = 1/2$) complexes with respect to the ground-state electronic structures of the Co^{II} and M^{II} ions. Some heterodinuclear complexes with low-spin Co^{II} are reported[7d,7e,8,10,11] but their magnetic properties are not fully elucidated.

This work relates to magnetic properties of $M^{II}Co^{II}$ complexes derived from a phenol-based macrocyclic ligand, $(L^{2;2})^{2-}$ (Fig. 1). The ligand has two dissimilar $N(amine)_2O_2$ and $N(imine)_2O_2$ metal-binding sites sharing two phenolic oxygen atoms. μ-Acetato-di-μ-phenolato-metal(II)cobalt(II) complexes (metal(II) = Fe^{II}, Co^{II}, Ni^{II}, Cu^{II}, Zn^{II}), $[FeCo(L^{2;2})(\mu\text{-AcO})(MeOH)]ClO_4$ (**1**) and $[MCo(L^{2;2})(\mu\text{-AcO})]ClO_4$ (M = Co (**2**), Ni (**3**), Cu (**4**), Zn (**5**)), have been derived ($[M_aM_b(L^{2;2})]^{n+}$ or 'M_aM_b complex' means that the M_a is bound to the $N(amine)_2O_2$ site and M_b to the $N(imine)_2O_2$ site). Spin-exchange interaction of the complexes is studied with respect to the electronic structures of the M^{II} and Co^{II} ions and the dinuclear $M^{II}Co^{II}$ core structure.

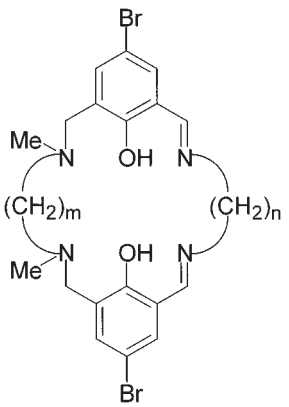

Fig. 1. Chemical structure of $H_2(L^{m;n})$.

Experimental

Physical Measurements. Elemental analyses of C, H, and N were obtained at The Service Center of Elemental Analysis of Kyushu University. Metal analyses were made using a Shimadzu AA-680 Atomic Absorption/Flame Emission Spectrophotometer.

† Present address: Graduate School of Engineering, Department of Synthetic Chemistry and Biological Chemistry, Kyoto University, Katsura, Nishikyo-ku, Kyoto 615-8510

Published on the web July 9, 2004; DOI 10.1246/bcsj.77.1343

Infrared spectra were measured using KBr disk on a PERKIN ELEMER Spectrum BX FT-IR system. Electronic absorption spectra in DMF were recorded on a Shimadzu UV-3100PC Spectrophotometer and X-Band EPR spectra were recorded on a JEOL JEX-FE3X spectrometer. Magnetic susceptibilities of powdered samples were measured on a Quantum Design MPMS XL SQUID susceptometer in the temperature range of 2–300 K. Diamagnetic corrections were made using Pascal's constants.[12] Magnetization studies were carried out using the same susceptometer at 2 K.

Preparations. The proligand, *N*,*N*′-dimethyl-*N*,*N*′-ethylenedi(5-bromo-3-formyl-2-hydroxybenzylamine) (H_2L'), was prepared by the literature method.[7] Syntheses of metal complexes were carried out in an atmosphere of nitrogen using a VAC globe box system of Nexus100026-S1 type.

$[PbCo(L^{2;2})(dmf)_4](ClO_4)_2$: The Co^{II} complex of H_2L', [Co(L′)], was prepared in situ by the reaction of H_2L' (5.00 g, 9.72 mmol) and cobalt(II) acetate tetrahydrate (2.43 g, 9.72 mmol) in acetonitrile (50 cm^3) at ambient temperature. $Pb(ClO_4)_2 \cdot 3H_2O$ (4.47 g, 9.72 mmol) was added to the solution of [Co(L′)], and an acetonitrile solution (10 cm^3) of ethylenediamine (0.584 g, 9.72 mmol) was dropped into the mixture with stirring. The resulting orange solution was concentrated to 30 cm^3 to afford a dark red precipitate. The yield was 10.3 g (90%). A portion was dissolved in DMF and the solution was diffused with 2-propanol to form reddish black crystals. Anal. Found: C, 31.54; H, 4.06; N, 8.66; Co, 4.44%. Calcd for $C_{34}H_{52}Br_2Cl_2CoN_8O_{14}Pb$: C, 31.56; H, 4.05; N, 8.66; Co, 4.56%. Selected IR data [KBr disk, ν/cm^{-1}]: 1649, 1445, 1143, 1087, 626.

$[FeCo(L^{2;2})(\mu\text{-OAc})(MeOH)]ClO_4$ (1): A solution of $[PbCo(L^{2;2})(dmf)_4](ClO_4)_2$ (500 mg, 0.386 mmol), iron(II) sulfate heptahydrate (107 mg, 0.386 mmol), and sodium acetate (35 mg, 0.425 mmol) in acetonitrile (100 cm^3) was refluxed for 2 h. The reaction mixture was filtered to separate $PbSO_4$ and the filtrate was evaporated to dryness. The residue was dissolved in methanol and the solution was diffused with diethyl ether to obtain reddish black crystals. They were separated by filtration and dried in air. The yield was 77%. Anal. Found: C, 35.71; H, 3.75; N, 6.62; Co, 7.48; Fe, 6.63%. Calcd for $C_{25}H_{31}Br_2ClCoFeN_4O_9$: C, 35.67; H, 3.71; N, 6.65; Co, 7.00; Fe, 6.63%. Selected IR data [ν/cm^{-1}] on KBr: 1625, 1606, 1579, 1552, 1446, 1293, 1110, 624. UV–vis [λ_{max}/nm (ε/$M^{-1}\,cm^{-1}$)]: 339 (8100), 428 (5340), ~550 (ca. 1500), and 1200 (14) in DMF.

$[CoCo(L^{2;2})(\mu\text{-OAc})]ClO_4$ (2): This was obtained as orange crystals in a way similar to that for **1** except for the use of cobalt(II) sulfate heptahydrate instead of iron(II) sulfate heptahydrate. The yield was 85%. Anal. Found: C, 35.26; H, 3.29; N, 6.82; Co, 14.28%. Calcd for $C_{24}H_{27}Br_2ClCoN_4O_8$: C, 35.47; H, 3.35; N, 6.89; Co, 14.50%. Selected IR data [ν/cm^{-1}] on KBr: 1610, 1567, 1447, 1296, 1084, 623. UV–vis [λ/nm (ε/$M^{-1}\,cm^{-1}$)]: 336 (6950), 408 (4850), ~530 (ca. 1000), and 1200 (14) in DMF.

$[NiCo(L^{2;2})(\mu\text{-OAc})]ClO_4$ (3): This was obtained as orange crystals in a way similar to that for **1** using nickel(II) sulfate hexahydrate. The yield was 83%. Anal. Found: C, 35.67; H, 3.41; N, 6.90; Co, 7.08; Ni, 7.23%. Calcd for $C_{24}H_{27}Br_2ClCoN_4NiO_8$: C, 35.48; H, 3.35; N, 6.90; Co, 7.25; Ni, 7.22%. Selected IR data [ν/cm^{-1}] on KBr: 1609, 1572, 1446, 1425, 1296, 1097, 1080, 623. UV–vis [λ/nm (ε/$M^{-1}\,cm^{-1}$)]: 333 (8000), 407 (4600), ~540 (ca. 560), and 1080 (9) in DMF.

$[CuCo(L^{2;2})(\mu\text{-OAc})]ClO_4$ (4): This was obtained as reddish black crystals using copper(II) sulfate pentahydrate. The yield was 80%. Anal. Found: C, 35.26; H, 3.41; N, 6.82; Co, 7.07; Cu, 7.18%. Calcd for $C_{24}H_{27}Br_2ClCoCuN_4O_8$: C, 35.27; H, 3.33; N, 6.86; Co, 7.21; Cu, 7.78%. Selected IR data [ν/cm^{-1}] on KBr: 1631, 1610, 1568, 1446, 1294, 1097, 623. UV–vis [λ/nm (ε/$M^{-1}\,cm^{-1}$)]: 348 (7600), 475 (1950), ~540 (ca. 850), and 740 (162) in DMF.

$[ZnCo(L^{2;2})(\mu\text{-OAc})]ClO_4$ (5): This was obtained as orange crystals using zinc(II) sulfate heptahydrate. The yield was 78%. Anal. Found: C, 35.01; H, 3.63; N, 6.55; Co, 6.56; Zn, 7.64%. Calcd for $C_{24}H_{27}Br_2ClCoN_4O_8Zn$: C, 35.19; H, 3.32; N, 6.84; Co, 6.92; Zn, 7.68%. Selected IR data [KBr disk, ν/cm^{-1}]: 1607, 1584, 1553, 1447, 1294, 1095, 623. UV–vis [λ/nm (ε/$M^{-1}\,cm^{-1}$)]: 339 (7000), 420 (5300), ~530 (ca. 1200), and 1270 (8) in DMF.

X-ray Crystallographic Analyses. Each single crystal of $[PbCo(L^{2;2})(dmf)_4](ClO_4)_2$ and the MCo complexes (**1**–**5**) was mounted on a glass fiber and coated with epoxy resin. All measurements were made on a Rigaku/MSC Mercury diffractometer with graphite monochromated Mo Kα radiation at -95 ± 1 °C. The data were corrected for Lorentz and polarization effects. Pertinent crystallographic parameters are summarized in Table 1.

The structures were solved by direct methods and expanded using Fourier techniques. The non-hydrogen atoms were refined anisotropically. Hydrogen atoms were included but not refined. Computations were carried out on a SGI O2 computer using teXsan crystallographic software package.[13]

Crystallographic data have been deposited at the CCDC, 12 Union Road, Cambridge CB2 1EZ, UK. Copies can be obtained on request, free of charge, by quoting the publication citation and the deposition numbers 214931–214936.

Results and Discussion

Synthesis and General Properties. The $M^{II}Co^{II}$ complexes of $(L^{2;2})^{2-}$ were synthesized by a stepwise template reaction developed in our laboratory.[6,14] The Co^{II} complex of *N*,*N*′-dimethyl-*N*,*N*′-ethylenedi(5-bromo-3-formyl-2-hydroxybenzylamine), [Co(L′)], was prepared and condensed with ethylenediamine in DMF in the presence of $Pb(ClO_4)_3 \cdot 3H_2O$ to afford the PbCo complex, $[PbCo(L^{2;2})(dmf)_4](ClO_4)_2$. The heterodinuclear complexes, $[FeCo(L^{2;2})(\mu\text{-AcO})(MeOH)]ClO_4$ (**1**) and $[MCo(L^{2;2})(\mu\text{-AcO})]ClO_4$ (M = Co (**2**), Ni (**3**), Cu (**4**), Zn (**5**)), were synthesized as good crystals when the PbCo complex was treated with M^{II} sulfate in acetonitrile in the presence of sodium acetate.

Previously, the transmetallation of Pb^{II} in $[PbCu(L^{2;2})](ClO_4)_2$ and $[PbCu(L^{2;3})](ClO_4)_2$ for a M^{II} ion resulted in the migration of the Cu^{II} from the $N(imine)_2O_2$ site to $N(amine)_2O_2$ site to afford $Cu^{II}M^{II}$ complexes.[7] Such metal migration is not the case in the present transmetallation reaction of $[PbCo(L^{2;2})(dmf)_4](ClO_4)_2$ with M^{II} sulfate, as discussed later.

The IR spectra of **1**–**5** show the ν_{as}(COO) and ν_s(COO) vibrations of acetate groups at 1584–1567 and 1447–1446 cm^{-1}, respectively.[15] The small separation between the two IR modes suggests a bridging function of the acetate group in each complex. Electronic absorption spectra of the complexes in DMF have an intense absorption band at 333–348 nm attributable to the π–π^* transition associated with the C=N linkage.[16,17] An absorption band at ~540 nm is characteristic of Co(salen) and related complexes.[18–20] Complexes **1**–**3** and **5** show a weak band at 1100–1200 nm that is assigned to a d–d band of the low-spin Co^{II}. This absorption is not resolved in the spectrum of **4**, owing to the more intense band at 740 nm; this is attributed to a superposed d–d band of Cu^{II}.

Table 1. Crystallographic Parameters for $[PbCo(L^{2;2})(dmf)_4](ClO_4)_2$ and the MCo Complexes (**1–5**)

	$[PbCo(L^{2;2})(dmf)_4](ClO_4)_2$	**1**	**2**	**3**	**4**	**5**
Formula	$C_{34}H_{52}Br_2Cl_2CoN_8O_{14}Pb$	$C_{25}H_{31}Br_2ClCoFeN_4O_9$	$C_{24}H_{27}Br_2ClCo_2N_4O_8$	$C_{24}H_{27}Br_2ClCoN_4NiO_8$	$C_{24}H_{27}Br_2ClCoCuN_4O_8$	$C_{24}H_{27}Br_2ClCoN_4O_8Zn$
Formula weight	1293.68	841.58	812.63	812.39	817.24	819.07
Crystal system	monoclinic	monoclinic	triclinic	triclinic	triclinic	triclinic
Space group	$P2_1/n$ (#14)	$P2_1/n$ (#14)	$P\bar{1}$ (#2)	$P\bar{1}$ (#2)	$P\bar{1}$ (#2)	$P\bar{1}$ (#2)
a/Å	13.901(4)	13.0196(9)	8.8921(2)	8.851(3)	8.891(2)	8.9005(2)
b/Å	23.935(6)	17.0466(8)	11.4225(2)	11.277(3)	11.342(3)	11.5254(1)
c/Å	14.637(4)	13.835(1)	14.8132(4)	14.828(5)	14.797(4)	14.8036(3)
α/°			77.177(7)	78.149(8)	77.544(6)	76.524(8)
β/°	109.726(3)	94.711(3)	81.640(8)	82.546(9)	82.473(7)	80.914(8)
γ/°			76.652(7)	77.320(8)	76.922(6)	76.124(7)
V/Å^3	4584.18	3060.08	1420.38	1407.54	1413.91	1425.28
Z value	4	4	2	2	2	2
D_{calcd}/g cm^{-3}	1.874	1.827	1.900	1.917	1.919	1.908
μ(Mo Kα)/cm^{-1}	59.71	37.79	41.39	42.56	43.23	43.84
Temperature/°C	−95	−95	−95	−95	−95	−95
p-factor	0.050	0.062	0.065	0.08	0.069	0.077
No. of reflections	10312	6847	6300	6282	6312	6241
R	0.076	0.051	0.053	0.064	0.057	0.048
R_w	0.109	0.100	0.098	0.135	0.111	0.107
Goodness of fit	0.75	1.00	1.02	1.00	1.00	1.00

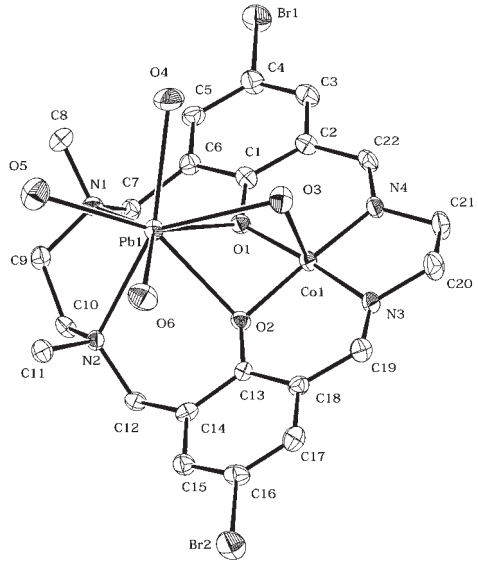

Fig. 2. An ORTEP drawing of the cationic part in $[PbCo(L^{2;2})(dmf)_4](ClO_4)_2$ with the atom numbering scheme. The dmf molecules are omitted for clarity except for the oxygen atoms O(3)–O(6).

Table 2. Selected Bond Distances (Å) and Angles (°) for $[PbCo(L^{2;2})(dmf)_4](ClO_4)_2$

Bond distances/Å			
Pb(1)–O(1)	2.542(4)	Pb(1)–O(2)	2.566(4)
Pb(1)–O(3)	2.787(2)	Pb(1)–O(4)	2.667(6)
Pb(1)–O(5)	2.711(5)	Pb(1)–O(6)	3.017(5)
Pb(1)–N(1)	2.520(4)	Pb(1)–N(2)	2.602(4)
Co(1)–O(1)	1.874(4)	Co(1)–O(2)	1.863(4)
Co(1)–O(3)	2.143(4)	Co(1)–N(3)	1.859(5)
Co(1)–N(4)	1.857(5)		
Bond angles/°			
O(1)–Pb(1)–O(2)	56.5(1)	O(1)–Pb(1)–N(1)	73.2(1)
O(1)–Pb(1)–N(2)	100.7(1)	O(2)–Pb(1)–N(1)	109.3(1)
O(2)–Pb(1)–N(2)	70.1(1)	N(1)-Pb(1)–N(2)	75.0(1)
O(1)–Co(1)–O(2)	80.6(2)	O(1)–Co(1)–N(3)	175.8(2)
O(1)–Co(1)–N(4)	95.8(2)	O(1)–Co(1)–O(3)	91.4(2)
O(2)–Co(1)–N(3)	95.2(2)	O(2)–Co(1)–N(4)	170.5(2)
O(2)–Co(1)–O(3)	91.9(2)	O(3)–Co(1)–N(3)	89.2(2)
O(3)–Co(1)–N(4)	96.9(2)	N(3)–Co(1)–N(4)	88.3(2)
Pb(1)–O(1)–Co(1)	94.4(1)	Pb(1)–O(2)–Co(1)	93.9(1)
Pb(1)–O(3)–Co(1)	40.44(9)		

Crystal Structures. $[PbCo(L^{2;2})(dmf)_4](ClO_4)_2$: An ORTEP[21] view of the complex is shown in Fig. 2 together with the atom numbering scheme. The selected bond distances and angles are given in Table 2.

The cation consists of the macrocycle $(L^{2,2})^{2-}$, Pb and Co ions and four dmf molecules; perchlorate ions are free from coordination and are captured in the crystal lattice. The Co^{II} is located in the $N(imine)_2O_2$ site and has a square-pyramidal geometry together with dmf oxygen (O(3)). The equatorial Co-to-donor bond distances range from 1.857(5) to 1.874(4) Å. The axial Co–O(3) bond distance is elongated (2.143(4) Å). The Co is displaced from the basal N_2O_2 least-squares plane by 0.078(3) Å toward the dmf oxygen.

The Pb ion in the $N(amine)_2O_2$ site has an eight-coordinate geometry together with four dmf oxygen atoms (O(3), O(4), O(5), and O(6)). One dmf molecule bridges the Co and Pb ions through its oxygen atom (O(3)). The Pb–O(3) and Co–O(3) bond distances are 2.787(4) and 2.143(4) Å, respectively. The Pb-to-macrocycle bond distances range from 2.520(4) to 2.602(4) Å. The Pb is displaced from N_2O_2 least-squares plane by 1.540(2) Å. The $N(imine)_2O_2$ least-squares plane and the $N(amine)_2O_2$ least-squares plane are bent at the O(1)···O(2) edge with a dihedral angle of 11.0(1)°. The intermetallic Co(1)···Pb(1) separation is 3.272(2) Å. The two *N*-methyl groups attached to N(1) and N(2) are situated *cis* with respect to the mean molecule plane.

The crystal structure of $[PbCu(L^{2;2})](ClO_4)_2$ is not determined but the structure of $[PbCu(L^{2;2})(BzO)(dmf)](ClO_4)_2$ ($BzO^- =$ benzoate) is known.[7a] The Pb has a seven-coordinate geometry together with a chelating BzO^- group and a dmf molecule. A noticeable geometrical feature of $[PbCo(L^{2;2})(dmf)_4](ClO_4)_2$ is the dmf bridge between the Pb^{II} and Co^{II} ions. Because of this reason, it is likely that the transmetallation reaction of $[PbCo(L^{2;2})(dmf)_4](ClO_4)_2$ with $M^{II}SO_4$ proceeds by a mechanism differing from that of $[PbCu(L^{2;2})](ClO_4)_2$ with $M^{II}SO_4$, affording the $M^{II}Co^{II}$ complexes (**1**–**5**) as demonstrated below.

$[FeCo(L^{2;2})(\mu\text{-OAc})(MeOH)]ClO_4$ (1): An ORTEP picture of **1** is shown in Fig. 3 together with the atom numbering scheme. The selected bond distances and angles are given in Table 3.

The cation has the Fe^{II} ion in the $N(amine)_2O_2$ site and the Co^{II} ion in the $N(imine)_2O_2$ site. An acetate group bridges the two metal ions affording μ-acetato-di-μ-phenolato-iron(II)-cobalt(II) core. The Fe···Co separation is 2.886(2) Å. The Fe has a five-coordinate geometry together with an acetate oxygen atom (O(3)). The geometry around the Fe is regarded as square-pyramidal; the parameter τ[22] discriminating square-pyramid ($\tau = 0$) and trigonal-bipyramid ($\tau = 1$) is 0.221. The equatorial

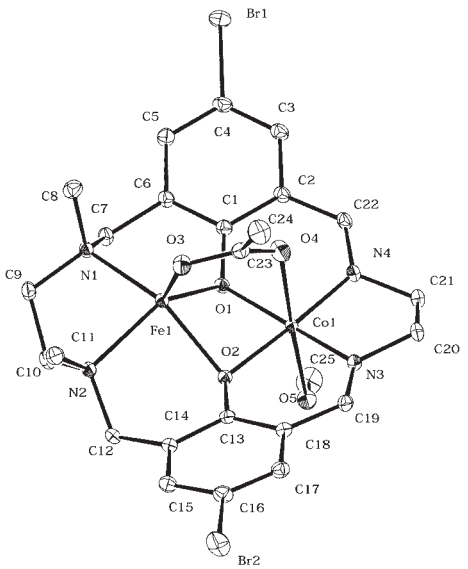

Fig. 3. An ORTEP drawing of the cationic part in $[FeCo(L^{2;2})(OAc)(MeOH)]ClO_4$ (**1**) with the atom numbering scheme.

Table 3. Selected Bond Distances (Å) and Angles (°) for $[FeCo(L^{2;2})(OAc)(MeOH)]ClO_4$ (**1**)

Bond distances/Å			
Co(1)–O(1)	1.913(2)	Co(1)–O(2)	1.881(2)
Co(1)–O(4)	2.408(2)	Co(1)–N(3)	1.874(2)
Co(1)–N(4)	1.853(2)	Co(1)–O(5)	2.242(2)
Fe(1)–O(1)	2.107(2)	Fe(1)–O(2)	2.098(2)
Fe(1)–O(3)	1.954(2)	Fe(1)–N(1)	2.171(2)
Fe(1)–N(2)	2.146(2)		
Bond angles/°			
O(1)–Fe(1)–O(2)	71.90(6)	O(1)–Fe(1)–N(1)	89.50(7)
O(1)–Fe(1)–N(2)	131.16(7)	O(2)–Fe(1)–N(1)	144.44(7)
O(2)–Fe(1)–N(2)	86.29(7)	N(1)–Fe(1)–N(2)	83.77(7)
O(1)–Co(1)–O(2)	81.21(7)	O(1)–Co(1)–N(3)	172.36(8)
O(1)–Co(1)–N(4)	95.43(8)	O(2)–Co(1)–N(3)	95.59(8)
O(2)–Co(1)–N(4)	176.64(8)	N(3)–Co(1)–N(4)	87.72(9)
Co(1)–O(1)–Fe(1)	91.63(7)	Co(1)–O(2)–Fe(1)	92.81(7)

Fe-to-donor bond distances range from 2.098(2) to 2.171(2) Å. The axial Fe–O(3) bond distance is 1.954(2) Å. The Fe is displaced from the $N(amine)_2O_2$ least-squares plane by 0.757(1) Å toward O(3).

The Co in the $N(imine)_2O_2$ has an axially-elongated octahedral geometry, together with the bridging acetate oxygen (O(4)) and a methanol oxygen (O(5)) at the axial sites. The equatorial bond distances range from 1.853(2) to 1.913(2) Å. The axial Co–O(4) and Co–O(5) bond distances are 2.408(2) and 2.242(2) Å, respectively.

The two *N*-methyl groups attached to N(1) and N(2) are situated *cis* with respect to the mean molecular plane. The $N(amine)_2O_2$ least-squares plane and the $N(imine)_2O_2$ plane are bent at the O(1)···O(2) edge with a dihedral angle of 23.56(5)°. Such bending of the dinuclear core with respect to the two basal planes is commonly recognized for dinuclear complexes of $(L^{2;2})^{2-}$ and $(L^{2;3})^{2-}$, irrespective of the nature of axial ligands, and is ascribed to steric requirements of the macrocyclic ligands.[7]

$[MCo(L^{2;2})(\mu\text{-OAc})]ClO_4$ (M = Co (2), Ni (3), Cu (4), Zn (5)): The crystals of these complexes are isomorphic. The structure of **2** is described in detail. An ORTEP view of **2** is shown in Fig. 4 together with the atom numbering scheme. The selected bond distances and angles are summarized in Table 4.

Complex **2** has a μ-acetato-di-μ-phenolato-dicobalt(II) core in the Co(1)···Co(2) intermetallic separation of 2.802(2) Å. The geometry around Co(1) bound to the $N(amine)_2O_2$ site is square-pyramidal ($\tau = 0.169$). The equatorial Co(1)-to-donor bond distances range from 2.006(2) to 2.095(2) Å and the axial Co(1)–O(3) bond distance is 1.953(2) Å. The Co(1) is displaced from the basal $N(amine)_2O_2$ least-squares plane by 0.547(1) Å toward O(3).

The geometry around Co(2) bound to the $N(imine)_2O_2$ site is also square-pyramidal ($\tau = 0.021$). The equatorial Co(2)-to-donor bond distances fall in the range of 1.852(2)–1.893(2) Å. The equatorial bond distances are significantly short relative to the Co(1)-to-donor bond distances. Instead, the axial Co(2)–O(4) bond distance (2.212(2) Å) is elongated relative to the Co(1)–O(3) distance. The Co(2) is displaced from the basal

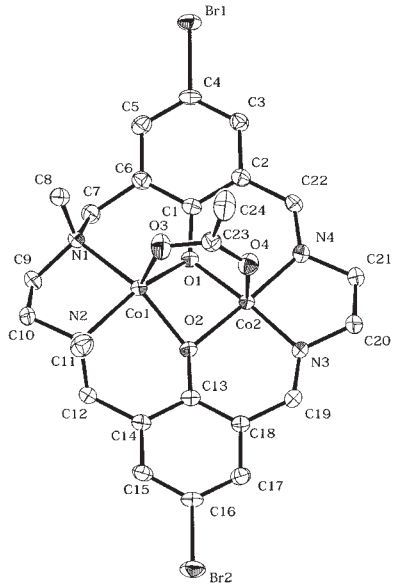

Fig. 4. An ORTEP drawing of the cationic part in $[CoCo(L^{2;2})(OAc)]ClO_4$ (**2**) with the atom numbering scheme.

Table 4. Selected Bond Distances (Å) and Angles (°) for $[CoCo(L^{2;2})(OAc)]ClO_4$ (**2**)

Bond distances/Å			
Co(1)–O(1)	2.066(2)	Co(1)–O(2)	2.006(2)
Co(1)–O(3)	1.953(2)	Co(1)–N(1)	2.080(2)
Co(1)–N(2)	2.095(2)	Co(2)–O(1)	1.882(2)
Co(2)–O(2)	1.893(2)	Co(2)–O(4)	2.212(2)
Co(2)–N(3)	1.852(2)	Co(2)–N(4)	1.860(2)
Bond angles/°			
O(1)–Co(1)–O(2)	73.67(6)	O(1)–Co(1)–N(1)	90.33(7)
O(1)–Co(1)–N(2)	153.47(7)	O(2)–Co(1)–N(1)	143.29(7)
O(2)–Co(1)–N(2)	92.09(7)	N(1)–Co(1)–N(2)	88.19(7)
O(1)–Co(2)–O(2)	80.62(6)	O(1)–Co(2)–N(3)	173.37(8)
O(1)–Co(2)–N(4)	95.26(7)	O(2)–Co(2)–N(3)	95.54(7)
O(2)–Co(2)–N(4)	174.67(8)	N(3)-Co(2)–N(4)	88.23(8)
Co(1)–O(1)–Co(2)	90.30(6)	Co(1)–O(2)–Co(2)	91.86(6)

$N(imine)_2O_2$ least-squares plane by 0.074(1) Å toward the acetate oxygen O(4). The $N(imine)_2O_2$ least-squares plane and the $N(amine)_2O_2$ least-squares plane are bent at the O(1)···O(2) edge with a dihedral angle of 25.79(5)°.

Geometrical characteristics of **1**–**5** are summarized in Table 5. All the complexes have a short mean Co–L_{eq} bond and a long axial Co–O(acetate) bond, in accord with the low-spin state of the Co^{II}.[23] The axial Cu–O(acetate) bond of **4** is long relative to the corresponding M–O(acetate) bond of other complexes. This is due to the Jahn–Teller effect for d^9 electronic configuration. A large displacement of the M^{II} from the basal $N(amine)_2O_2$ least-squares plane is recognized for **1** (M = Fe, 0.757(1) Å), **2** (Co, 0.547(1) Å), and **5** (Zn, 0.620(1) Å); the deviation of Ni in **3** is 0.399(2) Å and the deviation of Cu in **4** is 0.397(1) Å. The Co in **1** is displaced toward the methanol oxygen O(5) but not toward the acetate oxygen O(4). Because of this reason the Co–O(acetate) bond of **1** is elongated relative to the corresponding M–O(acetate) bond of other complexes.

Magnetic Properties. Magnetic susceptibilities of **1**–**5** were measured on a powdered sample in the temperature range of 2–300 K. Temperature-variations of the magnetic moments of **1**–**5** are given in Fig. 5. The magnetic property of **5** (ZnCo) is discussed first, because this is the simplest case among the complexes. It has a magnetic moment of 2.20 μ_B at room temperature. The moment monotonously decreased with decreasing temperature to 1.75 μ_B at 4 K, due to temperature-independent paramagnetism ($N\alpha$) associated with the Co^{II} ion. The $N\alpha$ value is estimated to be ca. 500×10^{-6} $cm^3\,mol^{-1}$ by the usual method to obtain constant $(\chi - N\alpha)T$ over the temperature range of 4–300 K. A similar $N\alpha$ value (ca. 460×10^{-6} $cm^3\,mol^{-1}$) is deduced for Co(salen).[24] Such a large $N\alpha$ value for low-spin Co^{II} may arise from low-lying excited states through a second-order Zeeman effect.

In order to determine the electronic configuration of the low-spin Co^{II}, we measured EPR spectrum of **5** (ZnCo) in a frozen DMF solution at liquid nitrogen temperature. The EPR spectrum is of axial pattern with $g_\perp = 2.25$, $g_\parallel = 2.02$, and $A_{Co} = 118 \times 10^{-4}$ cm^{-1}, demonstrating that one unpaired electron of the Co resides in its d_{z^2} orbital.[9]

The magnetic moment of **1** (FeCo) is 5.40 μ_B at room temperature; the moment decreased with decreasing temperature to 3.35 μ_B at 2 K. The cryomagnetic behavior suggests an antifer-

Table 5. Summary of Structural Characteristics of **1**–**5**

Complexes	**1**	**2**	**3**	**4**	**5**
Mean M–L_{eq}/Å	2.131	2.062	2.022	2.003	2.082
Mean Co–L_{eq}/Å	1.880	1.872	1.869	1.876	1.870
M–O(acetate)/Å	1.954	1.953	1.951	2.058	1.934
Co–O(acetate)/Å	2.408	2.212	2.189	2.205	2.222
M···Co/Å	2.89	2.80	2.81	2.81	2.86
δ for M/Å	0.757	0.546	0.399	0.397	0.621
δ for Co/Å	−0.060	0.074	0.077	0.094	0.063
τ for M	0.221	0.169	0.137	0.138	0.148
τ for Co	—	0.021	0.028	0.021	0.022
ρ/°	23.56	25.79	25.67	24.13	24.15

δ: Displacement of metal from basal N_2O_2 plane. τ: Parameter discriminating square-pyramid ($\tau = 0$) and trigonal-bipyramid ($\tau = 1$). ρ: Dihedral angle between $N(amine)_2O_2$ and $N(imine)_2O_2$ least-squares planes.

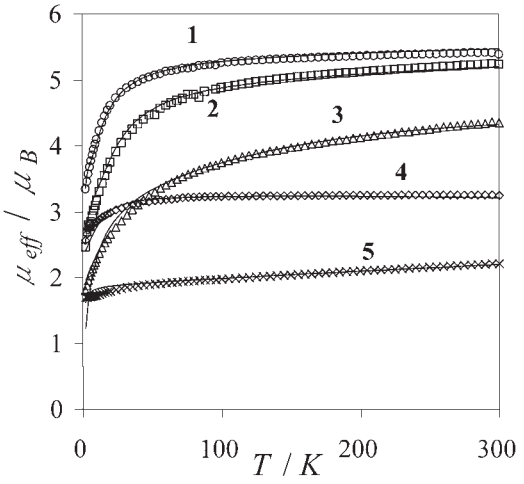

Fig. 5. Temperature-variations of magnetic moments of **1** (FeCo), **2** (CoCo), **3** (NiCo), **4** (CuCo), and **5** (ZnCo). The solid lines are best-fit curves based on respective treatments as discussed in the text.

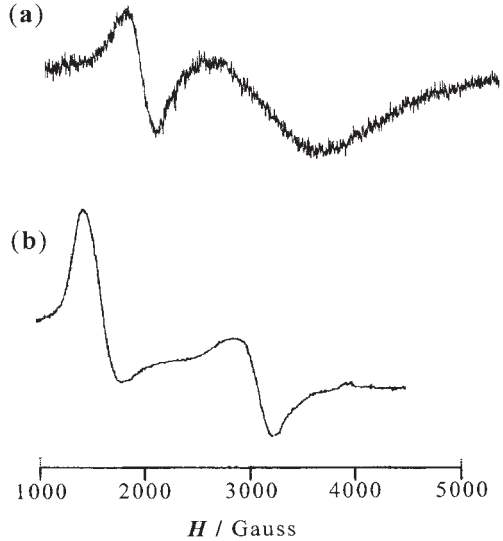

Fig. 6. EPR spectra of **3**; (a) on powdered sample at room temperature and (b) in frozen DMF solution at liquid nitrogen temperature.

romagnetic interaction between the Fe^{II} ($S = 2$) and Co^{II} ($S = 1/2$) ions. The magnetic moment at 2 K is smaller than the spin-only value for $S_T = 3/2$ (3.87 μ_B) arising from antiferromagnetic coupling of the metal ions. This fact indicates that the operation of some secondary effect such as zero-field splitting of the $S_T = 3/2$ term. The magnetic susceptibility expression for $Fe^{II}(S = 2)$–$Co^{II}(S = 1/2)$ based on the isotropic Heisenberg model $\boldsymbol{H} = -2J\boldsymbol{S}_1\boldsymbol{S}_2$ is given by Eq. 1,

$$\chi_M = \{5N\beta^2/4k(T-\theta)\} \times [7{g_{5/2}}^2 + 2{g_{3/2}}^2 \exp(-5J/kT)] /[3 + 2\exp(-5J/kT)] + N\alpha \quad (1)$$

where N is Avogadro's number, β is the Bohr magneton, k is the Boltzmann constant, J is the exchange integral, T is the absolute temperature, and $N\alpha$ is the temperature-independent paramagnetism. The θ is included as the correction term for any secondary magnetic contribution. $g_{5/2}$ and $g_{3/2}$ are g factors associated with the total spin states $S_T = 5/2$ and $3/2$, respectively, and are expressed using local g_{Fe} and g_{Co} factors as $g_{5/2} = (4g_{Fe} + g_{Co})/5$ and $g_{3/2} = (6g_{Fe} - g_{Co})/5$.[25,26] The cryomagnetic property of **1** is well simulated by Eq. 1 using the best-fit parameters of $J = -4.0$ cm^{-1}, $g_{Fe} = 2.07$, $g_{Co} = 2.17$, $\theta = -0.8$ K, and $N\alpha = 550 \times 10^{-6}$ cm^3 mol^{-1} (see Fig. 5). The $N\alpha$ value of $\sim 50 \times 10^{-6}$ cm^3 mol^{-1} for Fe^{II} seems reasonable from a survey of the literature.[27]

The magnetic moment of **2** (CoCo) at room temperature is 5.24 μ_B (per molecule) and the moment decreased with decreasing temperature to 2.46 μ_B at 2 K. Evidently, the Co^{II} in the $N(amine)_2O_2$ site is of high-spin and an antiferromagnetic interaction operates between the high-spin Co^{II} and the low-spin Co^{II} ions. Magnetic simulations were carried out using the magnetic susceptibility expression (2),

$$\chi_M = \{2N\beta^2/k(T-\theta)\} \times [5{g_2}^2 + {g_1}^2 \exp(-4J/kT)] /[5 + 3\exp(-4J/kT)] + N\alpha \quad (2)$$

where g_2 and g_1 are the g factors associated with the total spin states $S_T = 2$ and 1, respectively, and are expressed using local g_{Co1} (for high-spin Co) and g_{Co2} (low-spin Co) factors as $g_2 = (3g_{Co1} + g_{Co2})/4$ and $g_1 = (5g_{Co1} - g_{Co2})/4$. The cryomagnetic property of **3** is well reproduced by Eq. 2 using the magnetic parameters of $J = -8.0$ cm^{-1}, $g_{Co1} = 2.45$, $g_{Co2} = 2.17$, $\theta = -2.0$ K, and $N\alpha = 830 \times 10^{-6}$ cm^3 mol^{-1} (see Fig. 5). Again, the $N\alpha$ value of $\sim 330 \times 10^{-6}$ cm^3 mol^{-1} for high-spin Co^{II} seems reasonable from literature values.[27]

The magnetic moment of **3** (NiCo) is 4.35 μ_B at room temperature; this moment decreased with decreasing temperature to 1.80 μ_B at 2 K. Such cryomagnetic behavior cannot be explained by antiferromagnetic interaction between Ni^{II} ($S = 1$) and Co^{II} ($S = 1/2$) ions. In fact, the magnetic moment at room temperature is substantially larger than the value expected for magnetically isolated Ni^{II} ($S = 1$) and Co^{II} ($S = 1/2$) ions; a moment of 3.64–3.97 μ_B is predicted using $\mu_{Ni} = 2.9$–3.3 μ_B and $\mu_{Co} = 2.2$ μ_B (the moment for **5**). Such a large magnetic moment of **3** implies a ferromagnetic coupling affording $S_T = 3/2$ ground state, and this is supported by EPR studies (see Fig. 6). Two distinct EPR signals were observed around $\sim$2000 and $\sim$3100 gauss when EPR was measured on powdered sample at room temperature. It must be mentioned that high-spin Ni^{II} and low-spin Co^{II} show no EPR signal at room temperature. A similar EPR spectrum was obtained in a frozen DMF solution of **3** at liquid nitrogen temperature.

The decrease in magnetic moment with lowering temperature may result from a zero-field splitting D in the $S_T = 3/2$ ground state. The parallel and perpendicular magnetic susceptibilities χ_z and χ_x for $S = 3/2$ axially split in zero-field have been derived.[28] By taking into consideration the thermal population on the $S_T = 1/2$ state at the energy of $3J$, the magnetic susceptibility expressions are given as follows:

$$\chi_z = \{N\beta^2/4kT\} \times \{{g_{1/2}}^2 \exp(-3J/kT) + {g_{3/2}}^2[9\exp(-D/kT) + \exp(D/kT)]\} /\{\exp(-3J/kT) + \exp(-D/kT) + \exp(D/kT)\} \quad (3)$$

and

$$\chi_x = \{N\beta^2/4kT\} \times [{g_{1/2}}^2 \exp(-3J/kT) + {g_{3/2}}^2\{4\exp(D/kT) + (3kT/D)[\exp(D/kT) - \exp(-D/kT)]\}]/\{\exp(-3J/kT) + \exp(-D/kT) + \exp(D/kT)\} \quad (4)$$

and the susceptibility measured is given by $\chi_M = (\chi_z + 2\chi_x)/3$. D is the zero-field splitting parameter. $g_{1/2}$ and $g_{3/2}$ are the g factors associated with the spin states $S_T = 1/2$ and 3/2, respectively, and are expressed using local g_{Ni} and g_{Co} factors as $g_{1/2} = (4g_{Ni} - g_{Co})/3$ and $g_{3/2} = (2g_{Ni} - g_{Co})/3$.

Our preliminary magnetic analyses using Eqs. 3 and 4 indicated a very large positive J value ($J \geq 300$ cm^{-1}) and also a very large D value ($|D| \geq 150$ cm^{-1}), but the fitting in the temperature region below 100 K was poor. It must be noted that the magnetic moment at 2 K (1.80 μ_B) is much smaller than the expected moment from Eqs. 3 and 4 at 2 K ($\sim$3 μ_B). This fact means that some other effect is contributing to the cryomagnetic property of **3**. Eventually we have noticed that the dinuclear NiCo units are closely packed in the crystal with the nearest intermetallic Co···Co′ and Ni···Co′ separations of 5.98 and 6.84 Å, respectively (Fig. 7). Thus, we presume that an intermolecular antiferromagnetic interaction is operating in this complex.

In order to make a correction for the intermolecular interaction, the magnetic susceptibility expressions are modified as follows:

$$\chi_z = \{N\beta^2/4k(T-\theta)\} \times \{{g_{1/2}}^2 \exp(-3J/kT) + {g_{3/2}}^2[9\exp(-D/kT) + \exp(D/kT)]\} /\{\exp(-3J/kT) + \exp(-D/kT) + \exp(D/kT)\} \quad (3')$$

and

$$\chi_x = \{N\beta^2/4k(T-\theta)\} \times [{g_{1/2}}^2 \exp(-3J/kT) + {g_{3/2}}^2\{4\exp(D/kT) + (3kT/D)[\exp(D/kT) - \exp(-D/kT)]\}]/\exp(-3J/kT) + \exp(-D/kT) + \exp(D/kT)\}. \quad (4')$$

Using Eqs. 3′ and 4′, the cryomagnetic property of **3** can be simulated with $J = 300$ cm^{-1}, $|D| = 175$ cm^{-1}, $g_{Ni} = 2.35$, $g_{Co} = 2.40$, and $\theta = -15$ K (see Fig. 5).

A large zero-field splitting ($|D| \sim 175$ cm^{-1}) is remarkable. The zero filed splitting in $S_T = 3/2$ of $Ni^{II}Co^{II}$ ($S_{Co} = 1/2$) is induced by local anisotropy of Ni, dipolar interaction between Ni and Co, and antisymmetric interaction associated with a lowered symmetry of dinuclear NiCo core. Recently we reported an analogous $Ni^{II}Co^{II}$ ($S_{Co} = 1/2$) complex that exhibits a very small zero-field splitting.[29] It has a coplanar dinuclear core with respect to the equatorial $\{NiN_2O_2\}$ and $\{CoN_2O_2\}$ planes and shows little displacement of the metal from the basal N_2O_2 plane. Therefore, the large zero-field splitting in **3** may arise from antisymmetric interaction of the largely distorted NiCo core.

Because of the large zero-field splitting, the EPR signals observed are associated with the Cramers doublets ($M_S = \pm 1/2$). The signal at $\sim$3100 gauss is attributed to the resonance between $M_S = +1/2$ and $-1/2$ under applied field parallel to z axis and the signal around $\sim$2000 gauss can be the resonance under applied field perpendicular to the molecular axis. A large zero-field splitting in **3** is supported by magnetization studies (Fig. 8): the magnetization curve determined at 2 K is close to the Brillouin function for $S = 1/2$ but not $S = 3/2$. Based on these facts the sign of D is determined to be positive.

The magnetic moment of **4** (CuCo) is 3.25 μ_B at room temperature; the moment decreased with decreasing temperature to 2.56 μ_B at 2 K. Such magnetic behavior cannot be explained by antiferromagnetic interaction between Cu^{II} ($S = 1/2$) and Co^{II} ($S = 1/2$) ions. Judging from the room-temperature magnetic moment corresponding to two unpaired electrons, we suppose that a ferromagnetic coupling in this complex provides $S_T =$

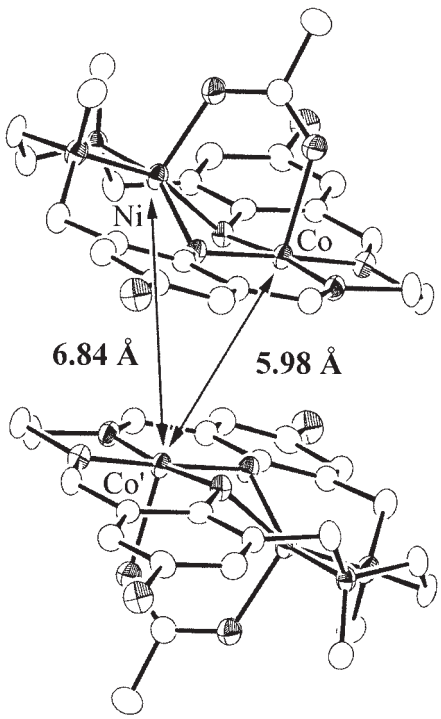

Fig. 7. The nearest interatomic Co–Co′ and Ni–Co′ separations in **5**.

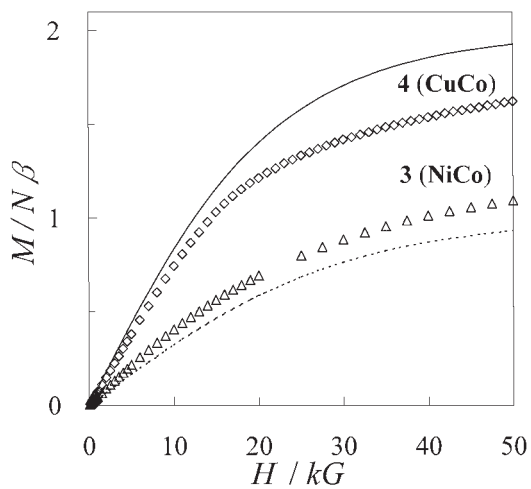

Fig. 8. Magnetization curves of **3** (NiCo) and **4** (CuCo) determined at 2 K. The solid and dotted lines are Brillouin functions for $S = 1$ and 1/2, respectively.

1 ground state. The decrease in magnetic moment with lowering temperature may arise from a zero-field splitting of the $S_T = 1$ state. By taking into consideration the thermal population on the $S_T = 0$ state at the energy of $2J$ and the axial zero-field splitting of the ground $S_T = 1$ state, the parallel and perpendicular magnetic susceptibility expressions are given as follows:[30]

$$\chi_z = \frac{2Ng_z^2\beta^2}{kT} \times \frac{\exp(-D/3kT)}{\exp(2D/3kT) + 2\exp(-D/3kT) + \exp(-2J/kT)} \quad (5)$$

$$\chi_x = \frac{2Ng_x^2\beta^2}{D} \times \frac{\exp(2D/3kT) - \exp(-D/3kT)}{\exp(2D/3kT) + 2\exp(-D/3kT) + \exp(-2J/kT)}. \quad (6)$$

Magnetic simulations were carried out by assuming $g_z = g_x$. The cryomagnetic property of **4** can be reproduced using a large positive J value ($J > 300$ cm^{-1}). In Fig. 5 is shown a best-fit curve using $J = 300$ cm^{-1}, $|D| = 30$ cm^{-1}, and $g = 2.30$.

In order to obtain a further support for the above magnetic analysis, we carried out magnetization studies for **4** (see Fig. 8). Occurrence of magnetization is unambiguous evidence for the ferromagnetic interaction between Cu^{II} and Co^{II} ions to afford the ground $S_T = 1$ state. The magnetization curve of **4** is close to the Brillouin function for $S = 1$, though it is hardly saturated, probably because of anisotropy of the complex.

From the above magnetic studies, an antiferromagnetic interaction occurs in **1** (FeCo) and **2** (CoCo), whereas a ferromagnetic interaction occurs in **3** (NiCo) and **4** (CuCo). Under square-pyramidal crystal field, the following ordering of d orbitals are supposed: $d_{xz}, d_{yz} < d_{xy} < d_{z^2} < d_{x^2-y^2}$. The electronic structure of the M^{II} in the N(amine)$_2$O$_2$ site is $(d_{xz})^2(d_{yz})^1(d_{xy})^1(d_{z^2})^1(d_{x^2-y^2})^1$ for Fe^{II}, $(d_{xz})^2(d_{yz})^2(d_{xy})^1(d_{z^2})^1(d_{x^2-y^2})^1$ for Co^{II}, $(d_{xz})^2(d_{yz})^2(d_{xy})^2(d_{z^2})^1(d_{x^2-y^2})^1$ for Ni^{II} and $(d_{xz})^2(d_{yz})^2(d_{xy})^2(d_{z^2})^2(d_{x^2-y^2})^1$ for Cu^{II}. The electronic structure of the low-spin Co^{II} is $(d_{z^2})^1$ as proved by the EPR study for **5** (ZnCo). The ferromagnetic interaction in **4** (CuCo) is interpreted by the strict orthogonality of magnetic orbitals, $d_{x^2-y^2}$(Cu) $\perp$ d_{z^2}(Co) (i.e., $J_{CuCo} = j(x^2 - y^2, z^2) > 0$).[31] The exchange integral for **3** is expressed using one-orbital exchange integrals as $J_{NiCo} = [j(x^2 - y^2, z^2) + j(z^2, z^2)]/2$. The $j(z^2, z^2)$ term must be negative but this contribution is smaller than that of the $j(x^2 - y^2, z^2)$ term since the J_{NiCo} integral is positive. The exchange integral of **1** is expressed as $J_{FeCo} = [j(yz, z^2) + j(xy, z^2) + j(z^2, z^2) + j(x^2 - y^2, z^2)]/4$ and that of **2** as $J_{CoCo} = [j(xy, z^2) + j(z^2, z^2) + j(x^2 - y^2, z^2)]/3$. Since the $j(yz, z^2)$ and $j(xy, z^2)$ terms are generally small,[31] one might expect a positive value for J_{FeCo} and J_{CoCo}. However, this is not the case of **1** and **2**. It appears that one of the antiferromagnetic contributions is enlarged in **1** and **2**. We presume that the large bend between the basal N(amine)$_2$O$_2$ and N(imine)$_2$O$_2$ planes and a large displacement of the M (Fe or Co) from the N(amine)$_2$O$_2$ plane give rise to an overlap between the d_{xy} orbital of the M^{II} and the d_{z^2} orbital of the Co^{II} as shown in Fig. 9.

In summary the heterodinuclear $M^{II}Co^{II}$ ($S_{Co} = 1/2$) complexes derived from $(L^{2;2})^{2-}$ exhibit antiferromagnetic interactions between the metal ions when M^{II} is Fe^{II} (**1**) or Co^{II} (**2**), whereas ferromagnetic interaction operates when M^{II} is Ni^{II} (**3**) or Cu^{II} (**4**). The ferromagnetic interaction in **3** and **4** results from the strict orthogonality of the magnetic orbitals, $d_{x^2-y^2}$(M) $\perp$ d_{z^2}(Co). The antiferromagnetic interaction in **1** and **2** is explained by d_{xy}(M) $\parallel$ d_{z^2}(Co) that is effected by a large bend between the basal N(amine)$_2$O$_2$ and N(imine)$_2$O$_2$ planes at the O···O edge ($\rho = 23.56°$ for **1** and 25.79° for **2**) and a large displacement of the M from the basal N(amine)$_2$O$_2$ plane (δ: 0.757 Å for Fe in **1** and 0.546 Å for Co in **2**). The geometrical distortion of the dinuclear core induces a large zero-field splitting in the $S_T = 3/2$ state of **3** ($D \sim 175$ cm^{-1}) and in the $S_T = 1$ state of **4** ($|D| = 30$ cm^{-1}).

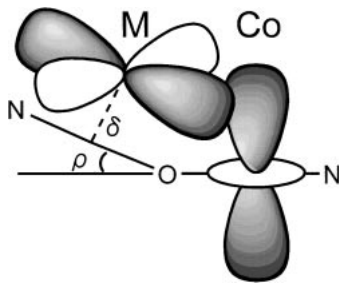

Fig. 9. Schematic representation of d_{xy}(M)–d_{z^2}(Co) overlap in **1** and **2**.

This work was supported by a Grant-in-Aid (No. 13640561) from the Ministry of Education, Culture, Sports, Science and Technology. One of the authors (M. Ohba) thanks Precursory Research for Embryonic Science and Technology (PRESTO), JST, for financial support.

References

1 O. Kahn, *Struct. Bonding*, **68**, 91 (1987).

2 S. J. Gruber, C. M. Harris, and E. Sinn, *J. Inorg. Nucl. Chem.*, **30**, 1805 (1968).

3 a) H. Ōkawa, Y. Nishida, M. Tanaka, and S. Kida, *Bull. Chem. Soc. Jpn.*, **50**, 127 (1977). b) N. Torihara, H. Ōkawa, and S. Kida, *Chem. Lett.*, **1978**, 1269.

4 a) O. Kahn, P. Tola, J. Galy, and H. Coudanne, *J. Am. Chem. Soc.*, **100**, 3931 (1978). b) O. Kahn, J. Galy, Y. Journaux, J. Jaud, and I. Morgenstern-Badarau, *J. Am. Chem. Soc.*, **104**, 2165 (1982).

5 S. L. Lambert, C. L. Spiro, R. F. Gagne, and D. N. Hendrickson, *Inorg. Chem.*, **21**, 68 (1982).

6 a) H. Ōkawa, J. Nishio, M. Ohba, M. Tadokoro, N. Matsumoto, M. Koikawa, S. Kida, and D. E. Fenton, *Inorg. Chem.*, **32**, 2949 (1993). b) S. Ohtsuka, M. Kodera, K. Motoda, M. Ohba, and H. Ōkawa, *J. Chem. Soc., Dalton Trans.*, **1995**, 2599. c) H. Wada, T. Aono, K. Motoda, M. Ohba, N. Matsumoto, and H. Ōkawa, *Inorg. Chim. Acta*, **246**, 13 (1996). d) T. Aono, H. Wada, M. Yonemura, H. Furutachi, M. Ohba, and H. Ōkawa, *J. Chem. Soc., Dalton Trans.*, **1997**, 3029. e) S. Kita, H. Furutachi, and H. Ōkawa, *Inorg. Chem.*, **38**, 4038 (1999).

7 a) M. Yonemura, Y. Matsumura, H. Furutachi, M. Ohba, H. Ōkawa, and D. E. Fenton, *Inorg. Chem.*, **36**, 2711 (1997). b) M. Yonemura, M. Ohba, K. Takahashi, H. Ōkawa, and D. E. Fenton, *Inorg. Chim. Acta*, **283**, 72 (1998). c) M. Yonemura, Y. Nakamura, N. Usuki, and H. Ōkawa, *Proc. Ind. Acad. Chem.*, **112**, 291 (2000).

d) M. Yonemura, N. Usuki, Y. Nakamura, and H. Ōkawa, *J. Chem. Soc., Dalton Trans.*, **2000**, 3624. e) M. Yonemura, K. Arimura, K. Inoue, N. Usuki, M. Ohba, and H. Ōkawa, *Inorg. Chem.*, **41**, 582 (2002).

8 O. Kahn, R. Claude, and H. Coudanne, *J. Chem. Soc., Chem. Commun.*, **1978**, 1012.

9 Y. Nishida and S. Kida, *Coord. Chem. Rev.*, **27**, 275 (1979).

10 H. Furutachi and H. Ōkawa, *Inorg. Chem.*, **36**, 3911 (1997).

11 S. Kita, H. Furutachi, and H. Ōkawa, *Inorg. Chem.*, **38**, 4038 (1999).

12 Landolt-Börnstein, Neue Series II/11, Springer-Verlag, Berlin (1981).

13 TEXSAN, Molecular Structure Corporation, Houston, TX, 1985 and 1992.

14 M. Tadokoro, H. Sakiyama, N. Matsumoto, M. Kodera, H. Ōkawa, and S. Kida, *J. Chem. Soc., Dalton Trans.*, **1992**, 313.

15 G. B. Deacon and R. J. Phillips, *Coord. Chem. Rev.*, **33**, 227 (1980).

16 B. Bosnich, *J. Am. Chem. Soc.*, **90**, 627 (1968).

17 R. S. Downing and F. L. Urbach, *J. Am. Chem. Soc.*, **91**, 5977 (1969).

18 a) H. Nishikawa and S. Yamada, *Bull. Chem. Soc. Jpn.*, **37**, 8 (1964). b) S. Yamada, *Coord. Chem. Rev.*, **1**, 415 (1966).

19 E. Cesarotti, M. Gullotti, A. Pasini, and R. Ugo, *J. Chem. Soc., Dalton Trans.*, **1977**, 757.

20 Y. Aratake, H. Ōkawa, E. Asato, H. Sakiyama, M. Kodera, S. Kida, and M. Sakamoto, *J. Chem. Soc., Dalton Trans.*, **1990**, 2941.

21 C. K. Johnson, Report 3794, Oak Ridge National Laboratory, Oak Ridge, TN, 1965.

22 A. W. Addison, T. N. Rao, J. Reedijk, J. V. Rijn, and G. C. Verschoor, *J. Chem. Soc., Dalton Trans.*, **1984**, 1349.

23 M. Calligaris, G. Nardin, and L. Randaccio, *Coord. Chem. Rev.*, **7**, 385 (1972).

24 B. N. Figgis and R. S. Nyholm, *J. Chem. Soc.*, **1959**, 338.

25 C. C. Chao, *J. Magn. Reson.*, **10**, 1 (1973).

26 R. P. Scaringe, D. J. Hodgson, and W. E. Hatfield, *Mol. Phys.*, **35**, 701 (1978).

27 B. N. Figgis and J. Lewis, *Prog. Inorg. Chem.*, **6**, 37 (1964).

28 O. Kahn, "Molecular Magnetism," VCH (1993), pp. 21–23.

29 K. Danjobara, Y. Mitsuka, Y. Miyasato, M. Ohba, and H. Ōkawa, *Bull. Chem., Soc. Jpn.*, **76**, 1769 (2003).

30 O. Kahn, "Molecular Magnetism," VCH (1993), pp. 17–21.

31 C. J. Cairns and D. H. Busch, *Coord. Chem. Rev.*, **69**, 1 (1986).